CFD Modeling of a Flat Plate

A.D.Thirumuruga (Roll No.10603035)

Paramita Das (Roll No. 10603045)

Department of Mechanical Engineering,

National Institute of Technology Rourkela,

Rourkela – 769008, India.

CFD Modeling of a Flat Plate

Project Report Submitted in partial fulfillment of the requirements for the degree of

Bachelor of Technology

in

Mechanical Engineering

By

A.D. Thirumuruga (Roll No.10603035)

Paramita Das (Roll No. 10603045)

National Institute of Technology Rourkela,

Rourkela – 769008, India.

May 2010

Acknowledgement

We would like to thank NIT Rourkela for giving us the opportunity to use their resources and work in such a challenging environment. First and foremost we take this opportunity to express our deepest sense of gratitude to our guide *Prof. S.Murugan* for his able guidance during our project work. This project would not have been possible without his help and the valuable time that he has given us amidst his busy schedule.

We would like to express my gratitude to Prof. R.K. Sahoo (Head of the Department) and Prof. K..P.Maity for their valuable suggestions and encouragements at various stages of the work.

We would also like to extend our gratitude to our friends and senior students of this department who have always encouraged and supported in doing our work. Last but not the least we would like to thank all the staff members of Department of Mechanical Engineering who have been very cooperative with us.

A.D.Thirumuruga

Paramita Das

ABSTRACT

Performance of an aircraft wing depends on the smoothness of the air flow over it. Any accumulation of frost, snow or ice on the wings or other horizontal surfaces will substantially alter the lifting characteristics of the airfoil and also changes the values of aerodynamic forces exerted on the airfoil. So any small change in flow parameters could affect its performance in a larger scale. This can sometimes be disastrous too. The wings of the airplane are also susceptible to corrosion also due to the excess humidity level. When it comes to large airfoils like aircraft wings, these parameters have to be maintained perfect so that the probability of failure is minimized. The basic test surface for investigating the effects of various parameters to the underlying boundary layer is the universal flat plate. Therefore a flat plate is used for this study.

The present paper concentrates on analyzing various flow parameters of cold air while it flows over a flat plate. Modeling and analysis of the flow were performed using FLUENT, version 6.3. The results obtained are purely the simulation software based calculations.

TABLE OF CONTENTS

LIST OF FIGURES

CHAPTER ONE

INTRODUCTION

According to the flight manual for the performance capabilities of an airplane are always related to standard atmosphere. However, rarely the airplane actually operates under conditions that approximate standard atmosphere. Any increase in temperature or altitude means a decrease in the aircraft's optimum performance.

MOTIVATION

Humidity plays an important part in flight conditions. High humidity has an effect on engine power. An accumulation of frost, snow or ice on the wings or other horizontal surfaces will substantially alter the lifting characteristics of the airfoil. Even a very light layer of frost spoils the smooth flow of air over the airfoil by separating the vital boundary layer air, producing an increase in stall speed and a decrease in stall angle of attack. It has been proven that a few millimetres of ice will increase the stall speed by as much as 20%. Any substantial accumulation of snow or ice, in addition to adding significantly to the weight of the airplane, so drastically disrupts the airflow over the wing, that the wing may not be able to develop lift at all. The wings of the airplane are also susceptible to corrosion also due to the excess humidity level. Examples where this high humidity level can affect are airliner fuselages and avionics, which can fail due to condensation of moist air on them. As the failure of either is potentially catastrophic, airliners operate with low internal relative humidity, often under 10%, especially on long flights. The low humidity is a consequence of drawing in the very cold air with a low absolute humidity, which is found at airliner cruising altitudes. Subsequent warming of this air lowers its relative humidity.

WORK OUTLINE

An experiment to understand the behaviour of airfoils in an air flow was conducted. Various parameters and their variation during the test conditions were evaluated. Forces acting on the airfoil during the test condition were calculated

CHAPTER TWO

AIRFOIL

An airplane wing has a special shape called airfoil or aerofoil which is in the shape of a wing or blade of a propeller, rotor or turbine. The forward part of the airfoil is rounded and is called the leading edge. The end part is narrow and tapered and is called the trailing edge. A reference line is used often for airfoils known as chord, an imaginary straight line joining the extremities of the leading edge and the trailing edge. There is a difference in the curvatures of the upper and lower surfaces of the airfoil (the curvature is called camber). The camber of the upper surface is more pronounced than that of the lower surface, which is somewhat flat in most instances. The distance from the chord line to the upper and lower surfaces of the wing denotes the magnitude of the upper and lower chamber at any point. Another reference line, drawn from the leading edge to the trailing edge, is the "mean camber line." This mean line is equidistant at all points from the upper and lower contours.

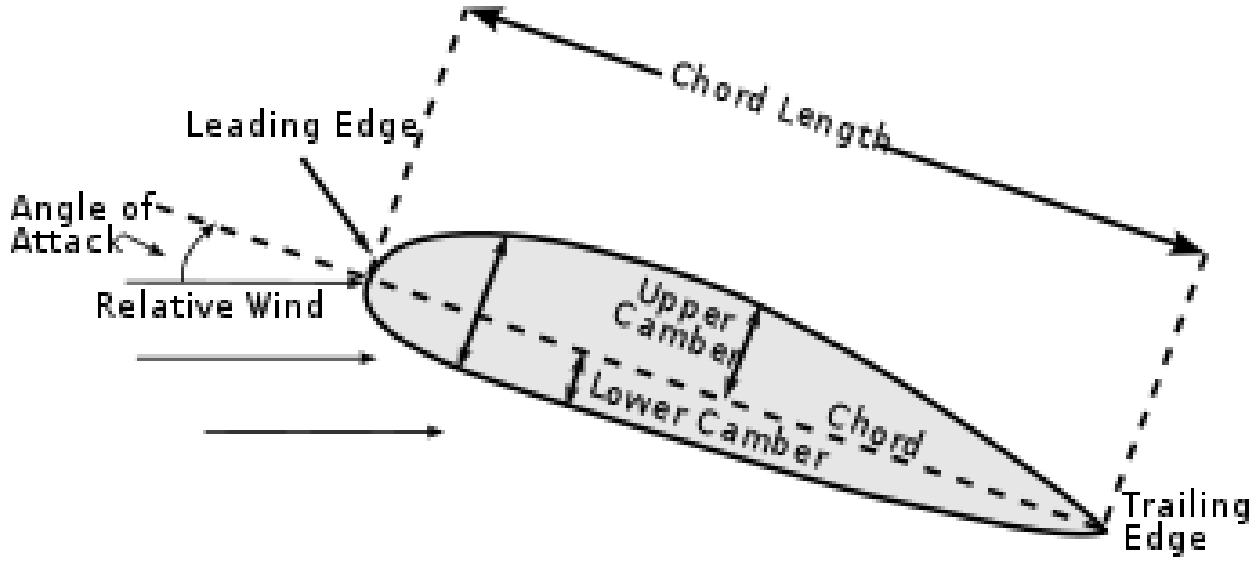

Fig 1: Nomenclature of an airfoil

As the airfoil moves through the air, the air is split and it passes over and below the wings. The airfoil when moves through a fluid produce a force perpendicular to the motion, called lift. It is primarily due to its shape and the angle of attack.

When either of them is positive, the flow field about the airfoil has a higher average velocity on the upper surface than on the lower one. This velocity difference is accompanied by a pressure difference, according to Bernoulli's principle for incompressible, in viscid fluid which produces the lift force. Bernoulli's theorem explains that with high velocity, pressure decreases and vice versa. The airfoil is designed in such a way that there is an increase in the airflow above its surface, thereby decreasing the pressure above the airfoil. Simultaneously the pressure below the airfoil is increased by the impact of the air on the lower surface. This combination of decreased air pressure above and increased air pressure below results in lift.

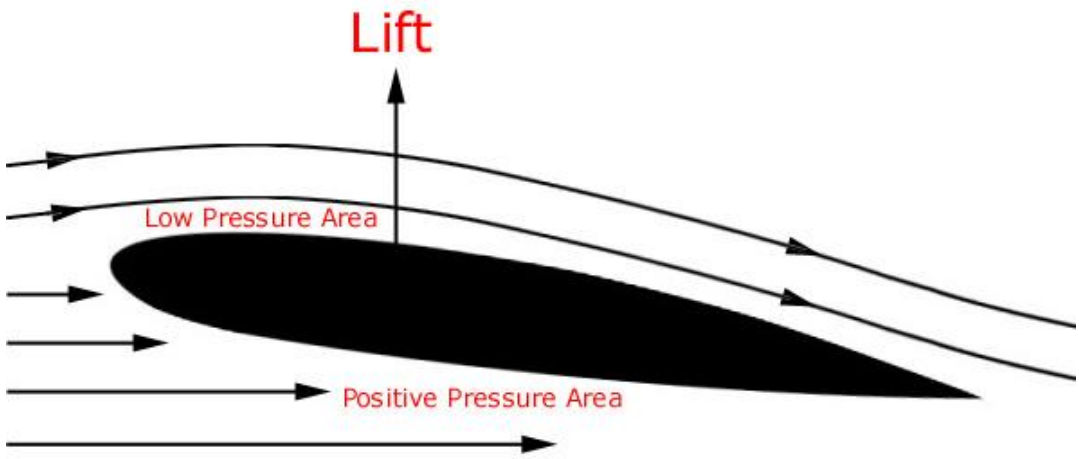

Fig 2: Forces exerted on the airfoil

Different airfoils have different flight characteristics. There are various types of airfoils suited for different flight regimes. The weight, speed, and purpose of each airplane dictate the shape of its airfoil. Asymmetric airfoils can generate lift at zero angle of attack. A symmetric airfoil suits frequent inverted flight as in aerobatic aero plane. Subsonic airfoils have a round leading edge which is actually insensitive to the angle of attack. Supersonic airfoils are more angular in shape and have a very sharp leading edge and are sensitive to angle of attack.

Some common shapes of airfoils are shown below.

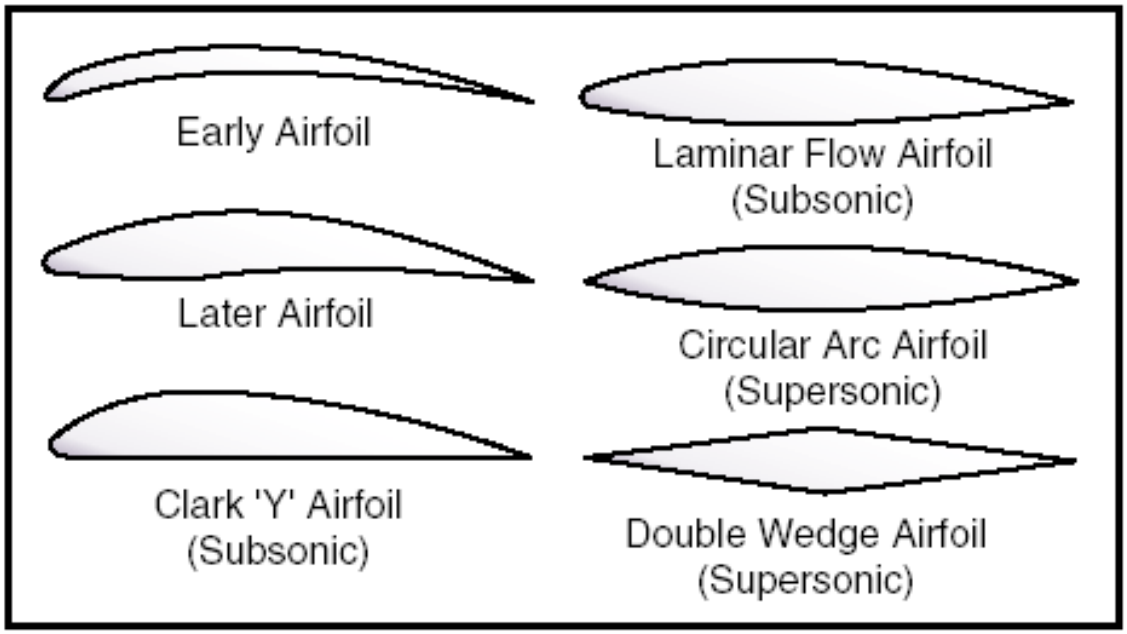

Fig 3: Types of airfoil

CONSTRUCTION OF AIRFOILS

In recent days, the construction of airfoils involves the use of philosophy of Richard eppler. It is a theoretical method to design an airfoil and to verify its performance. It involves a conformal mapping method for the design of airfoils with prescribed velocity distribution characteristics.

POTENTIAL FLOW AIRFOIL DESIGN METHOD

In this method, the velocity distribution is not specified at only one angle of attack. Instead, the input is the angles attack that will result in constant velocity over specified segments of the airfoil. Therefore, the input is a pair of parameters: the segment of airfoil and angle of attack relative to the zero lift line that will result in constant velocity over that segment.

At the trailing edge, a main pressure recovery is specified. Finally, a short closure contribution must be introduced to ensure that the trailing edge will be closed. In reality, the segments corresponding to the various input angles of attack are not specified in the airfoil plane but rather in the conformal-mapping plane in which the

airfoil is represented by a circle. No difficulties have arisen in correlating the arcs of the circle with the segments of the airfoil. An option has been included that allows a transition ramp to be specified by only two points, a forward and an aft limit, relative to the beginning of the pressure recovery. It should be remembered that for any given velocity distribution there does not necessarily exist a "normal" airfoil. For example, the closure contributions could be quite large, which would result in a very large trailing-edge angle. The closure contributions could also give rise to a region of negative thickness near the trailing edge. Accordingly, several iteration options have been included that allow the trailing-edge angle to be specified while certain input angles of attack or the amount of pressure recovery is iterated.

POTENTIAL-FLOW AIRFOIL ANALYSIS METHOD

The potential-flow airfoil analysis method employs panels with parabolic vorticity distributions. The geometry of the panels is determined by a spline fit of the airfoil coordinates, with the end points of the panels being the input airfoil coordinates themselves. The flow condition, which requires the inner tangential velocity to be zero, is satisfied at each airfoil coordinate (i.e., at the end points of the panels, not the midpoints). Two angles of attack, 0° and 90°, are analyzed. The flow at an arbitrary angle of attack is derived from these two solutions by superposition. The entire procedure does not require any restrictions on the input point distribution, smoothing, or rearranging of the coordinates; only the original airfoil coordinates are used.

An option is included by which additional points can be splined in between the original coordinates. This option allows more precise results to be obtained should a portion of the airfoil have a sparse distribution of points. An option is provided for smoothing airfoils. In addition, several options are available for the generation of coordinates for NACA 4-digit, 5-digit, and 6-series airfoils as wells FX (Workman) airfoils. A flap deflection can be introduced by geometrically rotating part of the airfoil about a flap-hinge point.

The connection between the forward portion of the airfoil and the flap is defined by an arc consisting of additional points that are generated automatically according to an input arc length. In addition, an option is included that allows the analysis of chord-increasing flaps. It should be noted that, while the airfoil shape that results from the exercise of this option does have an increased chord, it does not contain a slot and, therefore, is still a single-element as opposed to a multi element airfoil. An option is also provided for analyzing cascades. Boundary-Layer Method The laminar and turbulent boundary-layer development is computed using integral momentum and energy equations. The approximate solutions obtained from the laminar boundary-layer method agree very well with exact solutions. The turbulent boundary-layer method is based on the best available empirical skin-friction, dissipation, and shape-factor laws. Of special interest are the predictions of separation and transition. The

prediction of separation is determined by the shape factor based on energy and momentum thicknesses. (Note that this shape factor has the opposite tendency of the shape factor based on displacement and momentum thicknesses.) For laminar boundary layers, there exists a constant and reliable lower limit of this shape factor, which equals 1.515 and corresponds to laminar separation.

For turbulent boundary layers, no such unique and reliable limit exists. It has been determined, however, that the turbulent boundary layer will separate if the shape factor falls below 1.46 and will not separate if the shape factor remains above 1.58. It has also been determined that thicker boundary layers tend to separate at lower shape factors. The uncertainty is not a significant disadvantage because the shape factor changes rapidly near separation. Nevertheless, results must be checked carefully with respect to turbulent separation.

The prediction of transition is based on an empirical criterion that contains the Reynolds number, based on local conditions and momentum thickness, and the shape factor. Previously, the transition criterion used was a local criterion. Recently, a new empirical transition criterion has-been implemented that considers the instability history of the boundary layer. The results predicted using the new criterion is comparable to those using the en method but the computing time is negligible. The criterion contains a "roughness factor" that allows various degrees of surface roughness or free-stream turbulence to be simulated.

The prediction of transition results in as witch from the laminar skin-friction, dissipation, and shape-factor laws to the turbulent ones, without changing the shape factor or the momentum thickness. Also, a procedure has recently been incorporated into the code that empirically estimates the increase in the boundary-layer thickness due to laminar separation bubbles; this procedure yields an additional "bubble drag."

The code contains an option that allows the analysis of the effect of single roughness elements on a turbulent as well as a laminar boundary layer. For the laminar case, transition is assumed to occur at the position of the roughness element. This simulates fixing transition by roughness in a wind tunnel or in flight. The lift and pitching-moment coefficients are determined from the potential flow. Viscous corrections are then applied to these coefficients. The lift-curve slope where no separation is present is reduced to 2π from its theoretical value. In other words, the potential-flow thickness effects are assumed to be offset by the boundary-layer displacement effects. A lift-coefficient correction due to separation is also included. As an option, the displacement effect on the velocity distributions and the lift and pitching-moment coefficients can be computed. The boundary-layer characteristics at the trailing edge are used for the calculation of the profile -drag coefficient by acquire-Young type formula. In general, the theoretical predictions agree well with experimental measurements. (See ref. 3, for example.)The code contains an option that allows aircraft-oriented boundary-layer developments tube computed, where the

Reynolds number and the Mach number vary with aircraft lift coefficient and the local wing chord. In addition, a local twist angle can be input. Aircraft polars that include the induced drag and an aircraft parasite drag can also be computed.

LITERATURE REVIEW

1. **S.J. Karabelas and N.C. Markatos** studied the effect of water vapor condensation in forced convection flow over an airfoil.
   - The flow was considered subsonic and compressible at high Reynolds number.
   - Spalart – Allmaras model is used to account for the turbulence affect.
   - The study is based on a mixture two-phase model.
   - The phases may move at different velocities.

Humidity conditions affect the flight conditions at high altitudes. There is snow formation on the wings which affects the boundary layer flow and changes the aerodynamic forces. Most of the studies in this field are based on steady state nucleation theory for the vapor condensation which presumes that the appearance of a liquid phase in vapor depends on small clusters formed by fluctuations in the gaseous phase. These considerations are mainly based on the kinetic theory and correlations of the experimental data.

S.J Karabelas and N.C Markatos developed a new methodology where the water droplets were treated as a separate phase with different thermodynamic and flow properties. A two-mixture model was used with the mixture of air and water vapor or moist air being considered as the primary phase and the liquid water as the secondary. The phases exchange momentum and energy. The prominent part is though the mass transfer which determines the rate of formation of water droplets. The condensation is assumed to be at equilibrium. As soon as the saturation is reached, condensation starts. Droplets were considered spheres with diameter of 10^-5. The geometry examined was a Clark-y airfoil, bounded by two wall regions and another two fixed pressure type boundary conditions. The chord length of the airfoil was taken as 1 m. The effect of all the parameters is investigated for the upper part of the airfoil.

The results obtained are as follows:

- Mass fraction distribution for various humidity values:
  Four values of relative humidity were chosen- 50, 60, 70 and 85%. It was seen that for low humidity levels, the mass fraction was low. For all the humidity levels there is a peak after which the mass fraction is reduced gradually. At the trailing edge, the concentration is suppressed. For high relative humidity, the peak is closer to the trailing edge (position x=1).
- Mass fraction profile across the vertical line intersecting the trailing edge.

A maximum concentration is found to exist for every humidity value at about the same point (namely at 0.1 m above the trailing edge). It shows that when humidity level increases linearly, the relative positions of zero liquid concentrations move far from the airfoil exponentially. It confirms that the ambient humidity conditions strongly affect the momentum of water liquid and when the mass fraction of water vapor is significant in moist air, the droplets have enough energy and momentum to move far away from the source (regions of low temperature) towards all directions.The maximum mass fraction value is reached inside the trailing edge area and not on the suction side.

- Temperature distribution
  Lower temperatures were observed to exist at about 0.2 m far away from the leading edge, where there is no significant water liquid mass fraction. Near these regions of low temperature, the latter falls below the dew point and the cloud of liquid droplets begins to form.
- Rarefaction of the condensation cloud occurs quite smoothly. This is due to the large amount of energy and momentum that the secondary phase has already gained from the upstream regions, where the mass transfer rate was high. The liquid concentration vanishes after 10-15 m. the disappearance of the cloud was due to the loss of momentum and energy since no source exists beyond the airfoil.
- The boundary layer is much wider for high angle of attack due to considerable increase of crosswise momentum.
- Diagram of mass fraction values across the vertical line passing the trailing edge for all angles of attack. Between 0-2 degrees there is no significant difference in the width of the layer, which is because of the geometric shape of the airfoil. By increasing the angle, there was considerable increase in the liquid droplets' volume fraction.
- Relative humidity when upto 35% there is no generation of liquid phase. The flow is assumed to be single phase (moist air) and the only effect in the aerodynamic performance is a small change of density because of the difference in the vapor constitution. When humidity level is above 35%, the liquid phase is born and the effects become more pronounced.

2. **N.Patten, T.M. Young and P.Griffin** studied the design and characteristics of new test facility for flat plate boundary layer. Preliminary results for the test here are presented in the form of CFD, flow visualization, pressure measurements and thermal anemometry. The objective of the study was to design, manufacture and characterize a new flat plate for zero pressure gradient boundary layer research.

   The flat plate design comprised of a leading edge radius of 2mm with a 5 degree chamfer to the lower surface and a trailing edge adjustable flap designed for both positive and negative angles. The plate was made from 10 mm thick aluminium,

approximately 1 m by .290 m wide. 15 surface pressure measurement stations along the plate in the flow direction were placed. The static pressure was measured through 0.5 mm diameter holes on the surface which were connected to the manometer and allowed for the calculation of the static pressure along the working surface of the plate. The results obtained were as follows:

- From CFD analysis, the velocity vectors show that for a flap angle of 40 degree the stagnation point moves from the leading edge to the upper surface. The velocity contours show the stagnation point at the leading edge of the plate for a flap angle of 0 degree. It was also demonstrated that the boundary layer along the plate at zero incidence favorably follows the Blasius profile. The boundary layer formation is very much influenced by the shape of the leading edge of the plate and any pressure gradient that may be present in the flow.
- From flow visualization
  A mixture of powder particles and paraffin oil was utilized to observe the flow phenomenon over the plate. No adverse flow was allowed. It was found that with the flap at 40 degree, the leading edge separation was reduced significantly from approximately 10 mm to 3 mm which was obtained for 0 degree flap angle.
- Through thermal anemometry, it was shown that measurements along the flat plate compare favorably to the Blasius profile.
- Sufficient near wall resolution was confirmed due to the velocity profiles matching the linear law of the wall.
- Comparison between the experimentally measured boundary layer thickness, skin friction, frictional velocity and wall shear stress were found to deviate not more than 5% from the Blasius solutions.

CHAPTER THREE

EXPERIMENTAL SETUP

The set up designed for this experiment consists of an insulated cubical steel box with a glass cover on top. The cross section of the walls of the cubical box as shown in fig consists of a thermocol layer sandwiched between two steel sheets. At the two opposite sides of the cubical steel box, vents are provided for the entry and exit of moist air. The inlet vent is provided with a fan so as increase the striking air velocity. The exit vent which opens to the atmosphere, was closed with a thermocol plug after performing the experiment to insulate the apparatus from room conditions. The inner side of the box is provided with a platform to place the work piece.

Fig 4: Insulated cubical steel box

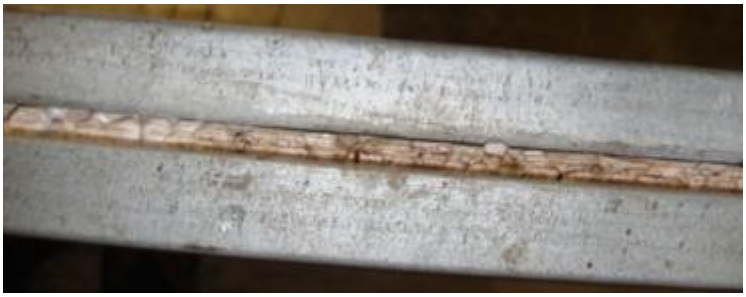

Fig 5: Cross section of the wall

An air conditioner was used as the cold air source. The air outlet is connected to the insulated box with pipes and GI funnels. The pipe and funnels were completely sealed using M-Seal. A thermometer was placed at the entry side of the moist air in order to record the inlet temperature of cold air. The exit temperature is also measured with a separate thermometer. A metal projection is fitted to the pipe so that I can be connected to the manometer for pressure measurement.

Fig 6: Cold air source - Air conditioner

Fig 7: GI funnels connecting the inlet vent

The pipe is attached to the funnel by a connector and it is packed by m-seal to prevent leakage of air. A hole is made on the pipe to which one end of the manometer pipe is inserted.

Fig 8 manometer

The work-piece to be tested in this experiment is a riveted joint, made by solid riveting two GI plates. This riveted joint is placed in line to the cold air inlet.

Fig 9: Work piece

Fig 10: Full arrangement of the apparatus

DIMENSIONS

Dimensions of the steel box: 132cm X 61 cm X 75 cm

Dimensions of the flat plate: 30 cm X 60 cm (riveted with pins at a distance of 3cm from each other)

Dimensions of the funnel: Overall Diameter - 31 cm

Bung Diameter – 5 cm

PROCEDURE

The work piece is placed on the platform so that the plate is in line with the inlet vent. Air conditioner and fan are switched on respectively. Inlet temperature and pressure were measured.

Fig 11: The inside of the steel box showing the work piece and the inlet vent

CHAPTER FOUR

OBSERVATION

CFD MODELLING

Computational Fluid Dynamics (CFD) is a standard tool in industry for analyzing external and internal flows of industrial devices. Examples where CFD is being used in the aeronautics industry are the prediction of lift and drag of airfoils and wings, flow around fuselages and entire aircrafts. On the engine side, CFD is used in the prediction of the performance and heat transfer in jet engines, including intakes, compressors, combustion chambers, turbines, and nozzles. Additional areas of application are internal flows in aircraft cabins, power supply units etc. Most industrial flows include turbulent flow structures that cannot be resolved numerically on available computers. To overcome the resolution limitations, CFD codes usually solve the Reynolds-Averaged Navier-Stokes equations augmented by turbulence models to compute the averaged turbulent stresses. These models are often the limiting aspect in the accuracy of numerical simulations. Close to solid structures or walls, boundary layers exist which typically require a high grid resolution and a special treatment in the numerical methods because of the steep velocity gradients.

The conditions of this experiment were simulated using FLUENT 6.3

A two dimensional model of the apparatus was created using GAMBIT.

Initial conditions

Inlet temperature: 20 degree Celsius

Inlet pressure: 2 atm

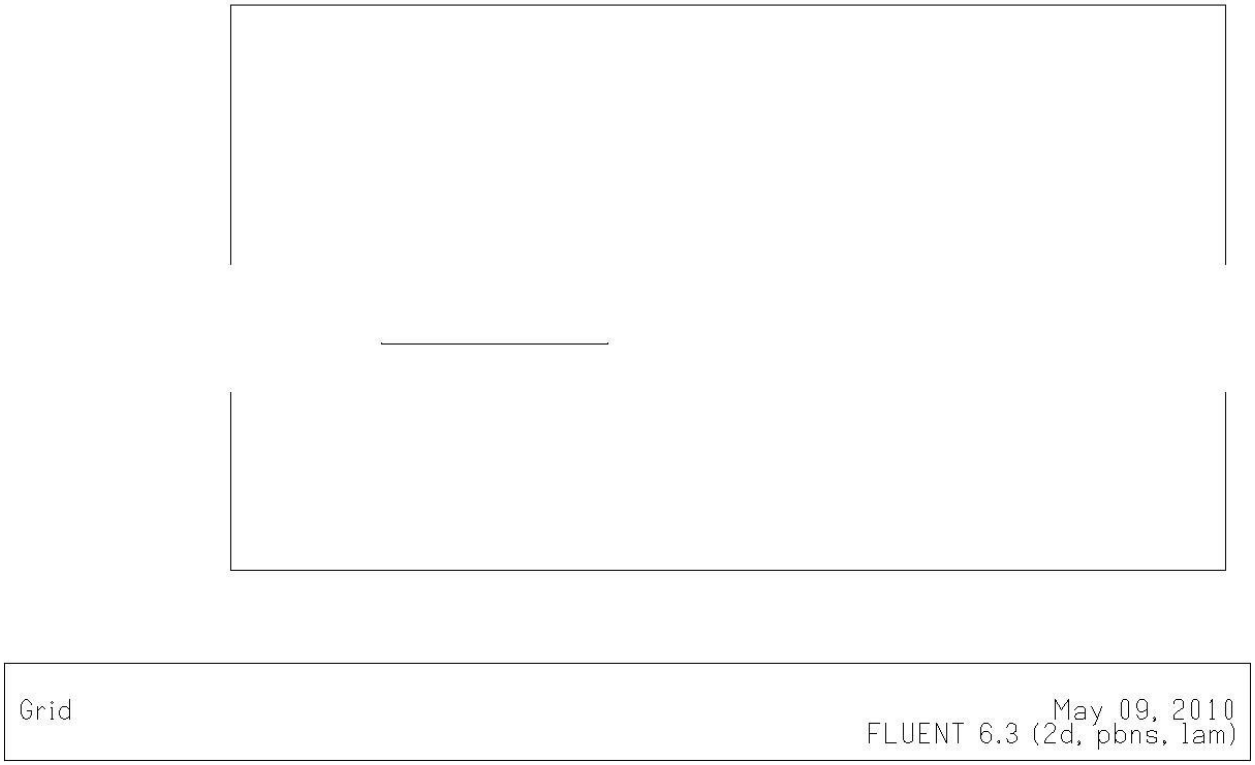

Fig 12: two dimensional models of the apparatus.

The outer walls shown in this figure is the apparatus in which the experiment was conducted. The work piece under experimentation is shown as a rectangle in between. The left vent is the opening for air inlet and right vent opens to the atmosphere. The apparatus is assumed to maintain an adiabatic condition i.e., the outer walls are insulated. The flow is considered completely laminar. No external heat is supplied to the work piece.

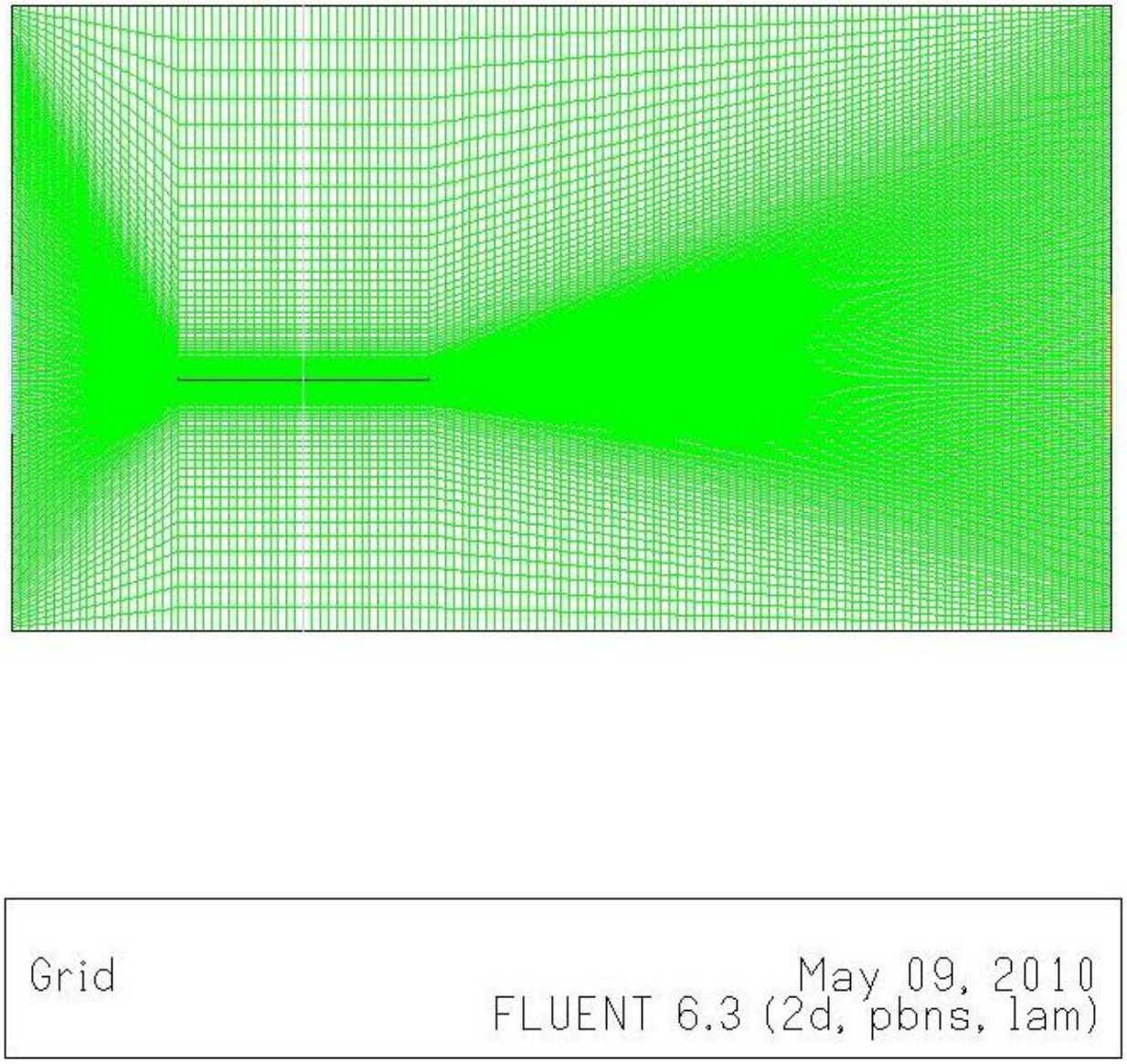

Fig 13: grid system

Fig 13 shows the grid generated for the analysis of a flat plate. Grid density was varied according to the necessity. Grid density is made the highest near the plate and the flowing region. All other areas of the model have a lesser grid density as the emphasis is given mainly on analyzing the changes near the plate.

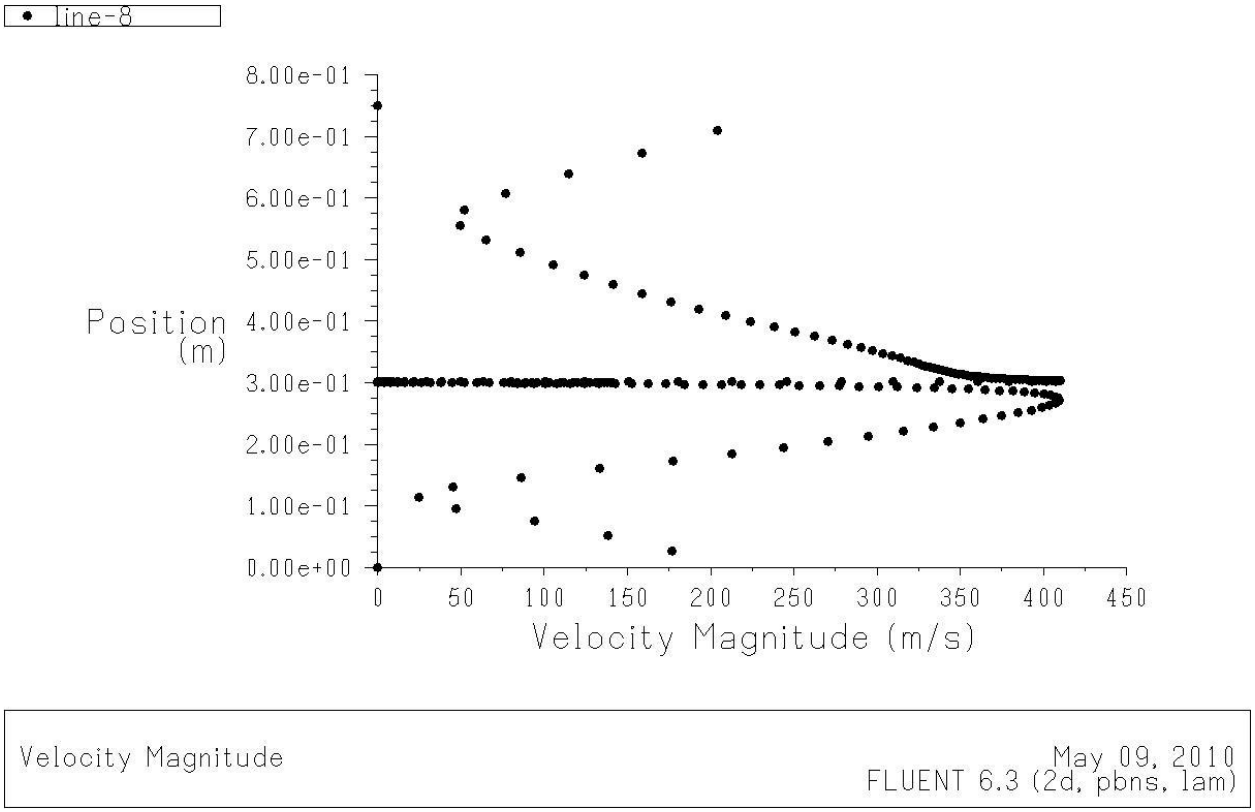

Fig 14: velocity variation in vertical direction

In Fig 14, the straight line obtained at the y coordinate 3.00e-01 represents the plate position where the velocity magnitude undergoes negligible amount of change. The points obtained above the straight line refer to the velocity variation with the vertical distance above the plate. The points obtained below the straight line refer to the velocity variation with the vertical distance below the plate. It is observed that the velocity remains maximum near the plate. Along the vertical direction the velocity decreases as the distance from the plate increases. This is observed both above and below the plate. Also after a particular distance from the plate the velocity magnitude again increases and saturates at a point.

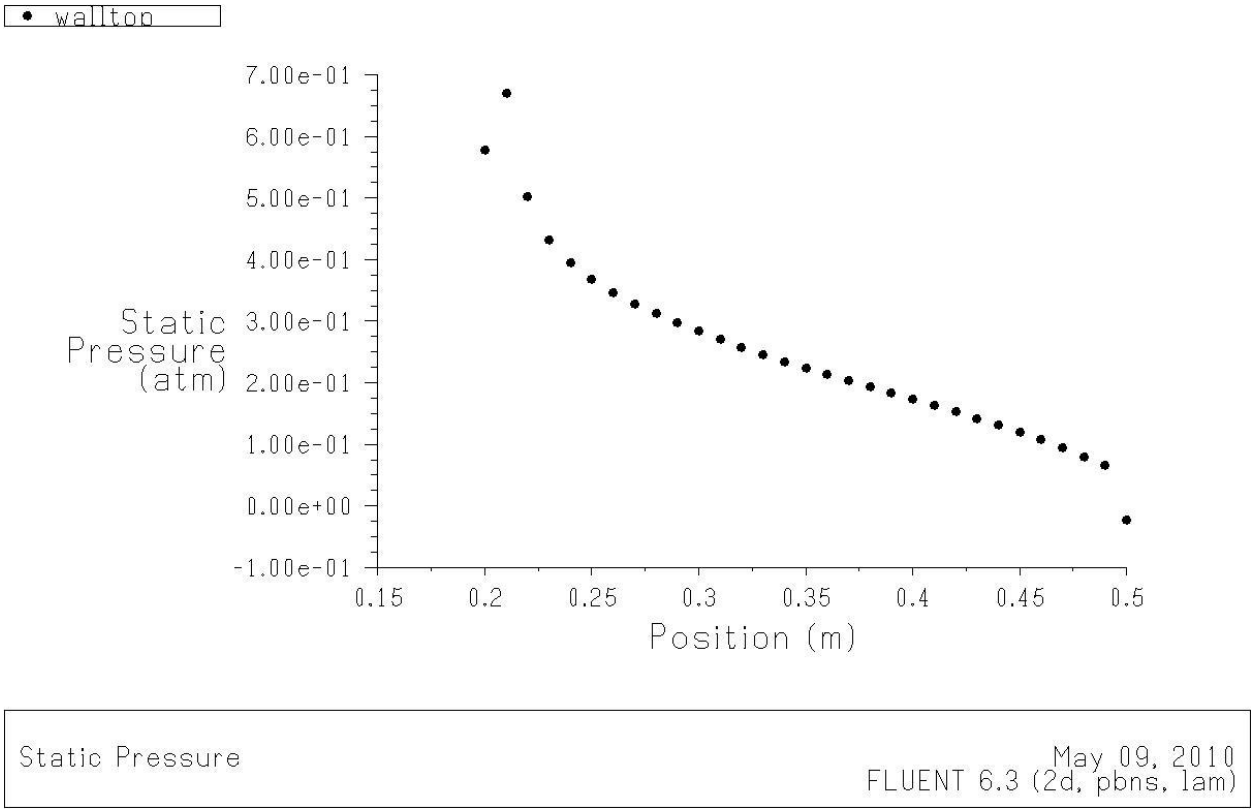

Fig 15: static pressure variation along the length of the plate

Fig 15 shows the variation of static pressure with the plate length. It's observed that the pressure is maximum at the initial position i.e., the left wall of the plate. On moving along the plate's length it decreases slowly to reach the minimum by the end of the plate.

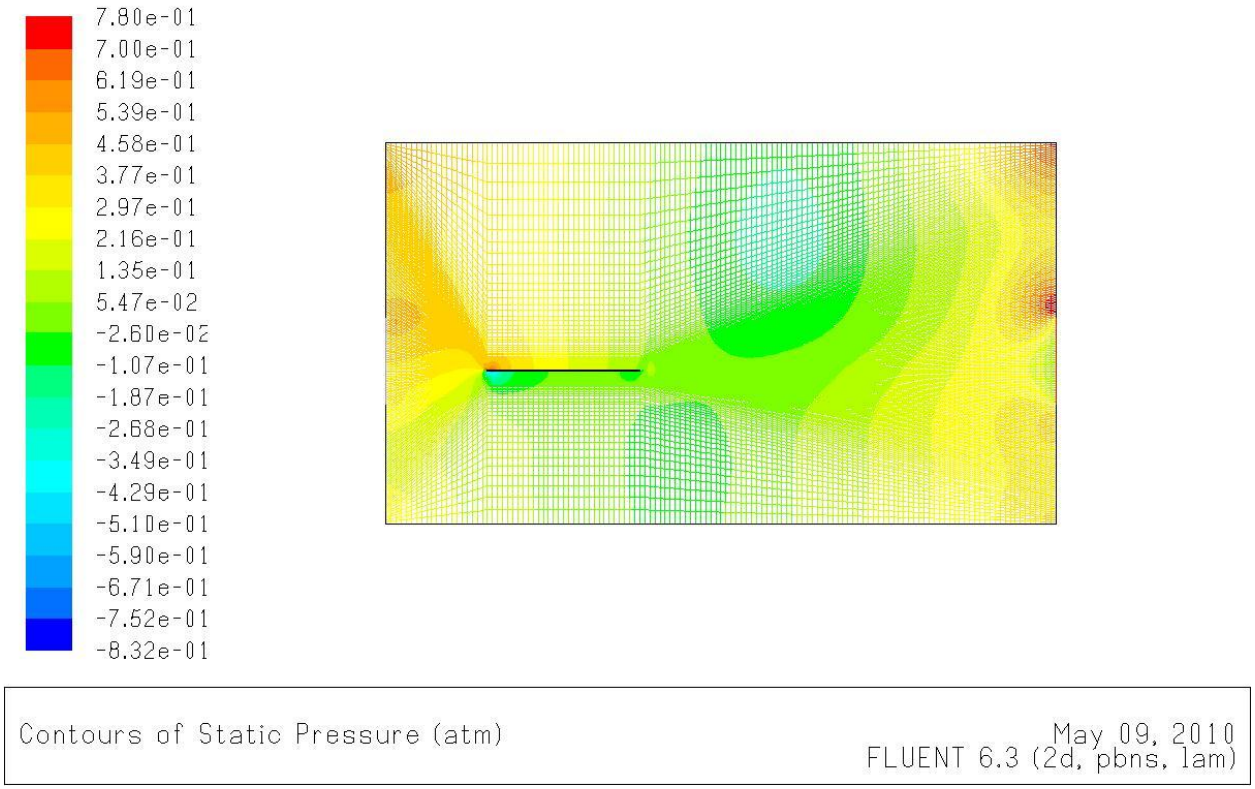

Fig 16: contour of static pressure

Fig 16 shows the pressure contour inside the apparatus. From the color scale, it can be inferred that pressure remains constant and distributed before it strikes the plate (yellow shade). After the plate has been struck, velocity decreases and varies on moving along the plate (yellow to green on moving along the plate length). A considerable amount of pressure drop has been observed on the top surface of the plate. It is noted that the pressure drop reaches its maximum in the left side of the bottom wall (aqua colored shade at the leftmost point of the bottom surface). The value goes as low as -5.10 e-01. Pressure drops more on the bottom surface than the top surface.

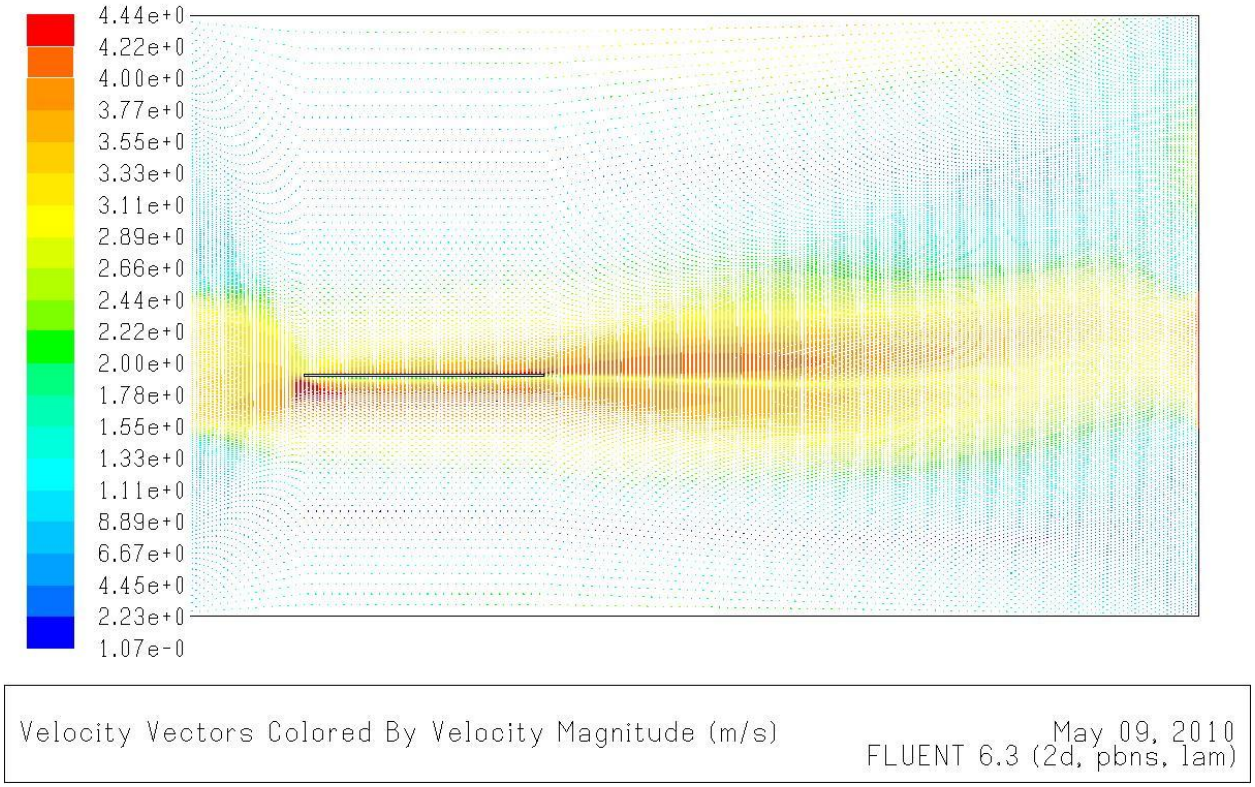

Fig 17: velocity vectors colored by velocity magnitude

Fig 17 shows the velocity vector contour inside the apparatus. As observed from the plot, velocity remains constant before striking the plate (shown by a yellow shade). After striking the plate, velocity goes on increasing along the length of the plate. At the trailing edge, velocity reaches the maximum value obtained above the plate. On considering the bottom surface of the flat plate, velocity is maximum at the leftmost point i.e., the point at which cold air strikes the plate (brown shade of the contour). Contrary to the top surface, velocity decreases along the plate length on the bottom surface.

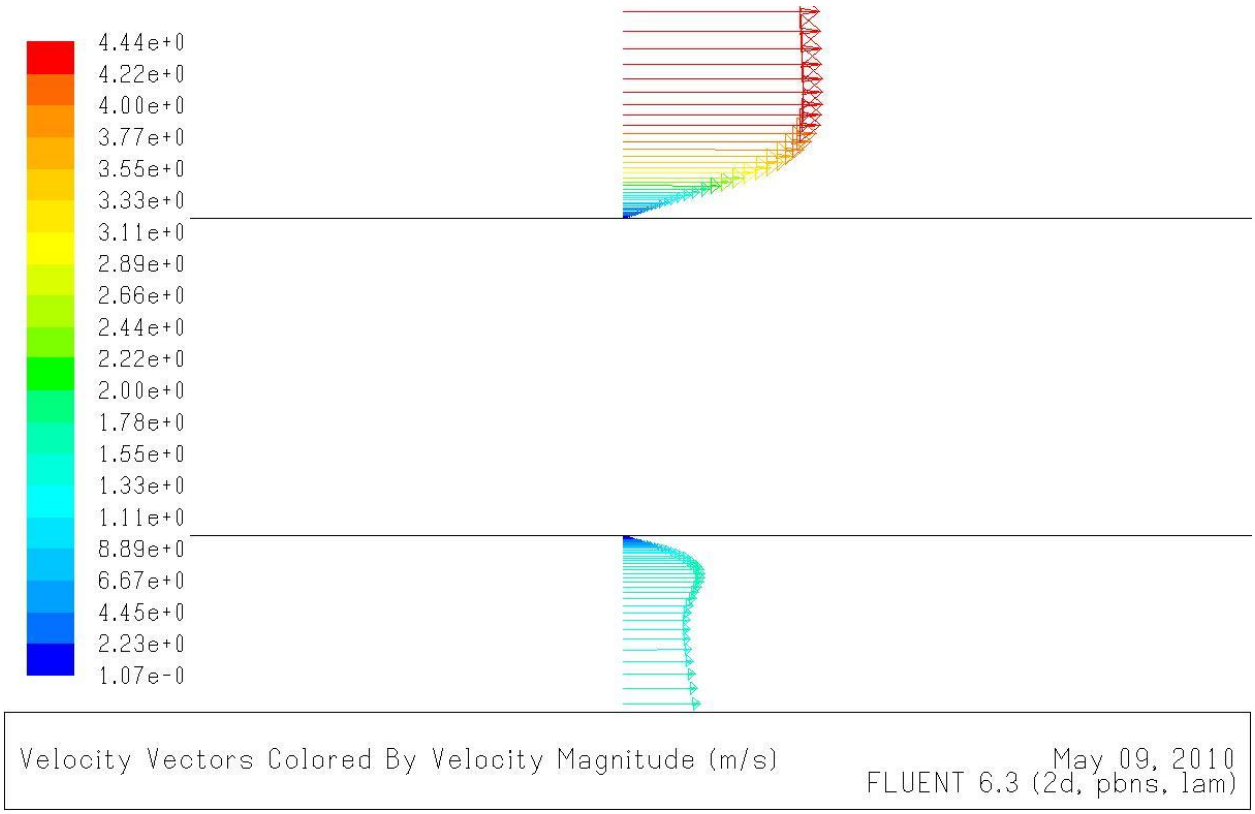

Fig 18: velocity vectors colored by velocity magnitude

Fig 18 shows the velocity variation with the vertical distance from the plate. Boundary layer formation is clearly visible on the top surface of the plate. This states that the flow above the plate is laminar. When the bottom surface is considered, velocity increases from zero, then decreases after the peak value. Velocity again increases and gets saturated at a certain distance from the plate. This shows that the flow below the flat plate is both laminar and turbulent.

CHAPTER FIVE

RESULTS

The following values were computed with the available input data.

Table 1: **Horizontal component of forces acting on the plate**

Zone name	**Pressure force (in N)**	**Viscous force (in N)**	**Total force (in N)**	**Pressure coefficient**	**Viscous coefficient**	**Total coefficient**
Wall bottom	0	11.18541	11.18541	0	18.261893	18.261893
Wall left	68.339478	0.0027328045	68.34221	111.57466	0.0044617217	111.57912
Wall right	15.337138	0.0027931198	15.339931	25.040226	0.0045601955	25.044786
Wall top	0	9.0182486	9.0182486	0	14.723671	14.723671
Net	83.676616	20.209184	103.8858	136.61488	32.994586	169.60947

Table 2: **Vertical component of forces acting on the plate**

Zone name	**Pressure force (in N)**	**Viscous force (in N)**	**Total force (in N)**	**Pressure coefficient**	**Viscous coefficient**	**Total coefficient**
Wall bottom	-2518.5183	-.042073216	-2518.5604	-4111.8666	-0.068690965	-4111.9353
Wall left	0	-0.0015914305	-0.001591430	0	-0.002598253	-0.002598253
Wall right	0	0.0043588621	0.0043588621	0	0.0071165095	0.0071165095
Wall top	-7713.8584	-0.015108398	-7713.8735	-12594.055	-0.024666773	-12594.079
Net	-10232.377	-0.054414183	-10232.431	-16705.921	-0.088839482	-16706.01

Table 3: **Various parameters at the inlet and outlet**

Parameter	**Inlet**	**Outlet**	**Net**
Heat transfer rate (w)	-345722.34	345680	-42.34375
Area weighted average static pressure (in atm)	0.38320631	0	0.19160315
Area weighted average static temperature (in K)	293	293.00079	293.0004
Area weighted average static velocity (in m/s)	311.99713	326.34314	319.17014
Mass flow rate (in Kg/s)	11.875409	-66.703743	-66.703743

CONCLUSIONS

From the above analysis, the conclusions have been made.

1. When the top surface of the plate is considered, air velocity increases on moving along the plate's length. This reaches the maximum at the trailing edge of the plate.
2. Considering the bottom surface of the plate, contrary to the top surface, air velocity decreases along the plate's length. Also the maximum velocity is obtained at the leading edge of the plate. This value is higher than the maxima at the top surface.
3. Above the test piece, air velocity increases with increase in distance from the plate in the vertical direction. This value becomes constant after a certain distance from the plate in vertical direction. Hence the flow over the plate is laminar.
4. Below the test piece, air velocity increases and decreases with the vertical distance from the plate. It first increases, reaches the peak, then decreases to the minima and again increases. Hence the flow below the plate is turbulent.
5. On the top surface, Static pressure of the flowing cold air decreases along the plate length. It is at its maximum at the leading edge and decreases to reach the minima at the trailing edge.
6. At the bottom surface, pressure drops at the trailing edge and reaches its minima after which it slowly increases. Pressure drops again at the trailing edge.
7. The pressure drop at the bottom surface of the plate causes water vapor condensation over the bottom surface. This corrodes and weakens the riveted joint. A possible solution for this is to place a heating element in strips all along the riveted joint.
8. Heat transfer rate, static pressure, static temperature, static velocity and mass flow rate at the inlet and outlet have been computed.
9. Horizontal and vertical components of pressure force, viscous force and net force acting over different faces of the plate were calculated.

REFERENCES

1. S.J.Karabelas and N.C. Markatos, Water vapor condensation in forced convection flow over an airfoil, aerospace science and technology, volume 12, issue 2, March 2008, pages 150-158.
2. N. Patten, T. M. Young, and P. Griffin , Design and Characteristics of New Test Facility for Flat Plate Boundary Layer Research, World Academy of Science, Engineering and Technology 58, 2009.
3. P.R. Spalart, S.R. Allmaras, one-equation turbulence model for aerodynamic flows, Technical Report AIAA-92-0439, American Institute of Aeronautics and Astronautics, 1992.
4. **Robert H.** Kraichnan, Pressure Fluctuations in Turbulent Flow over a Flat Plate, J. Acoust. Soc. Am. Volume 28, Issue 3, pp. 378-390 (May 1956)**.**
5. **A**F Messiter, Boundary-Layer Flow Near the Trailing Edge of a Flat Plate, *SIAM Journal on Applied Mathematics*, Vol. 18, No. 1 (Jan., 1970), pp. 241-257**.**